Soft-Templating Synthesis of Mesoporous Magnetic $CuFe_2O_4$ Thin Films with Ordered 3D Honeycomb Structure and Partially Inverted Nanocrystalline Spinel Domains

Christian Reitz,[a] Christian Suchomski,[a] Jan Haetge,[a] Thomas Leichtweiss,[a] Zvonko Jagličić,[b] Igor Djerdj,[c] and Torsten Brezesinski*[a]

Electronic Supplementary Information

Experimental methods

Materials

$Cu(NO_3)_2{\cdot}3H_2O$ (99.999 %), $Fe(NO_3)_3{\cdot}9H_2O$ (99.99 %), $LiClO_4$ (battery grade, 99.99 %), ethanol, and 2-methoxyethanol were purchased from ABCR, Sigma-Aldrich, and Acros Organics, respectively. $H[(CH_2CH_2)_{0.67}(CH_2CHCH_2CH_3)_{0.33}]_{89}(OCH_2CH_2)_{79}OH$, referred to as KLE (B. Smarsly, D. Grosso, T. Brezesinski, N. Pinna, C. Boissiere, M. Antonietti, C, Sanchez, *Chem. Mater.* 2004, **16**, 2948; D. Grosso, C. Boissiere, B. Smarsly, T. Brezesinski, N. Pinna, P. A. Albouy, H. Amenitsch, M. Antonietti, C. Sanchez, *Nat. Mater.* 2004, **3**, 787), was obtained from BASF SE and used as the structure-directing agent.

Synthesis of mesoporous $CuFe_2O_4$ thin films

In a water-free container, 40 mg of KLE dissolved in a mixture of 1.5 mL of ethanol and 0.5 mL of 2-methoxyethanol are combined with both 91 mg of $Cu(NO_3)_2{\cdot}3H_2O$ and 304 mg of $Fe(NO_3)_3{\cdot}9H_2O$. Once the solution is homogeneous, thin films can be produced via dip-coating on polar substrates, including quartz and polished Si(100) wafers. Optimal conditions include relative humidities below 10 % and constant withdrawal rates of 1-10 mm/s. For best results, the films are first aged at 250 °C for 12 h and then annealed in air using a 40 min ramp to 650 °C (J. Haetge, C. Suchomski, T. Brezesinski, *Inorg. Chem.* 2010, **49**, 11619).

Characterization

Transmission electron microscopy (TEM) and scanning electron microscopy (SEM) images were taken with a CM30-ST microscope from Philips and a LEO Gemini 982, respectively. Wide-angle X-ray diffraction (WAXD) measurements were carried out on an X'Pert PRO diffractometer from PANalytical instruments. Grazing incidence small-angle X-ray scattering (GISAXS) data were collected at the German synchrotron radiation facility HASYLAB at DESY on beamline BW4 using a MarCCD area detector and a sample-detector distance of ~1820 mm. X-ray photoelectron spectroscopy (XPS) spectra were acquired on a VersaProbe PHI 5000 Scanning ESCA Microprobe from Physical Electronics with monochromatic Al-Kα X-ray source and a hemispherical electron energy analyzer. The electron takeoff angle to the sample surface was adjusted to 54°. The C1s signal from adventitious hydrocarbon at 284.8 eV was used as the energy reference to correct for charging. Krypton physisorption measurements were conducted at 87 K using the Autosorb-1-MP automated gas adsorption station from Quantachrome Corporation. Optical absorption measurements were carried out on a Perkin Elmer Lambda 900 UV-vis-NIR spectrophotometer. A substrate made from fused silica and an aluminium mirror served as the reference for transmission and reflection measurements, respectively. Thermogravimetric analysis (TGA) data were obtained with a Netzsch STA 409 PC at a heating rate of 5 °C/min. The thermobalance was coupled to a Balzers QMG 421 quadrupole mass spectrometer. The ionization energy was 70 eV. The film thickness was determined with an Alpha Step IQ Surface Profiler from KLA Tencor. For crystal structure visualization, the software Crystal Impact Diamond version 3.2g was used.

Magnetization measurements were carried out on a Quantum Design MPMS-XL-5 superconducting quantum interference device (SQUID) magnetometer. Magnetization as a

function of temperature was measured in the range of 2-380 K with an applied field of 100 Oe. Magnetization as a function of field was measured up to a maximum field of 50 kOe.

For photodegradation experiments, 12 mL of an aqueous solution of 35 μmol/L Rhodamine B (RhB) combined with 0.1 mL of H_2O_2 (30 %) was irradiated with 254 nm light (P = 8 W) in the presence of a ~230 nm thick, KLE-templated $CuFe_2O_4$ spinel film with a total area of ~4 cm^2. 254 nm light was used for experimental reasons.

Electrochemical experiments were carried out in an argon filled JACOMEX glove box (O_2 < 0.5 ppm, H_2O < 1 ppm) in a three-electrode cell using an Autolab PGSTAT302 potentiostat. A lithium foil several times the area of the working electrode was used as the counter electrode; the reference electrode was a lithium wire. The electrolyte solution was 1.0 mol/L $LiClO_4$ in propylene carbonate. Galvanostatic charge/discharge measurements were conducted on 170 nm thick $CuFe_2O_4$ spinel films to study the electrochemical behavior using cutoff voltages at 3.5 V and 1.5 V vs. Li/Li^+. The weight was calculated by directly measuring the thickness and porosity of the thin film materials.

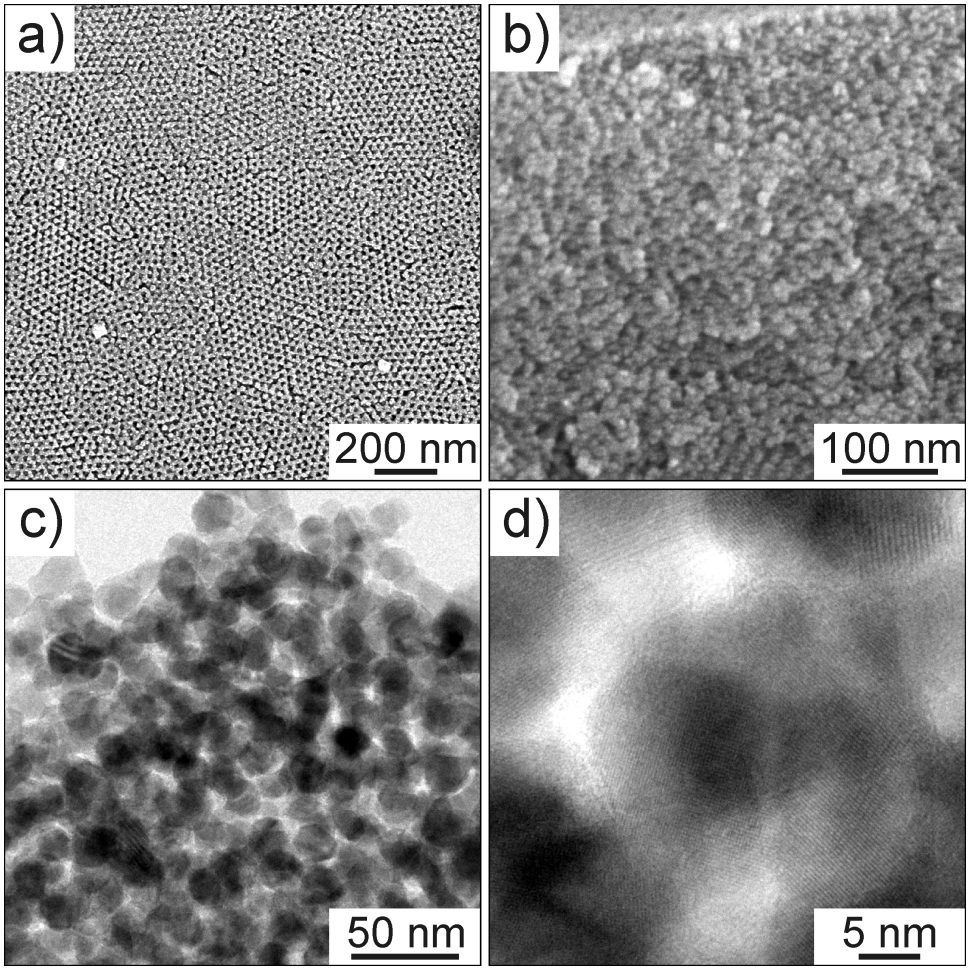

Figure S1. Morphology and nanoscale structure of KLE-templated $CuFe_2O_4$ spinel thin films heated to 650 °C. (a) Low-magnification SEM image showing open 17 nm diameter pores at the hexagonal top surface. (b) Cross-sectional SEM image showing that the pores persist throughout the bulk of the films. It is evident from the data in panels (a) and (b) that the materials studied in this work are both homogeneous and crack-free on the micrometer length scale after conversion of the initially amorphous pore walls to tetragonal $CuFe_2O_4$ spinel. (c) TEM image showing individual nanocrystalline spinel domains. (d) HRTEM image confirming the nanocrystallinity of the mesoporous $CuFe_2O_4$ thin films.

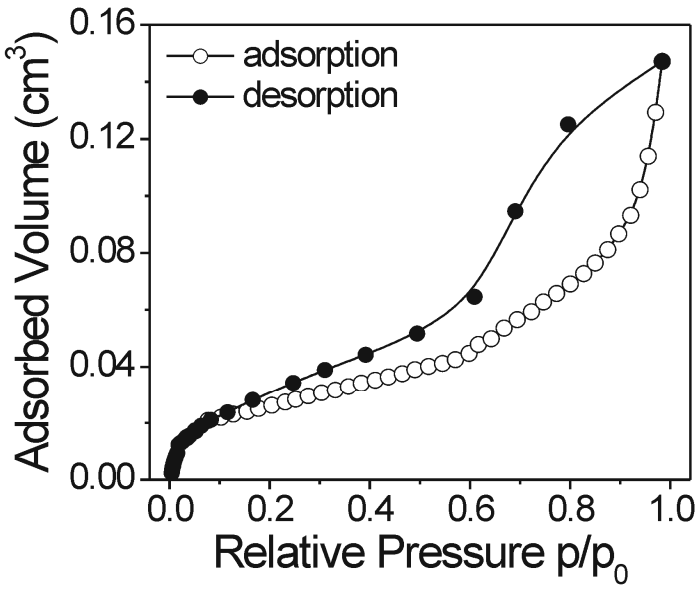

Figure S2. Krypton physisorption isotherms of ~175 nm thick, KLE-templated $CuFe_2O_4$ spinel films with a total area of 41 cm^2 heated to 650 °C. A porosity of ~30 % is obtained from these experiments, which is characteristic of KLE-templated oxide thin film materials. We estimate the error margin as being ±10 %. The reason for the use of krypton at 87 K over nitrogen at 77 K is the higher sensitivity of this technique - the saturation pressure of krypton at 87 K is only ~13 Torr (equivalent to 17.3 hPa).

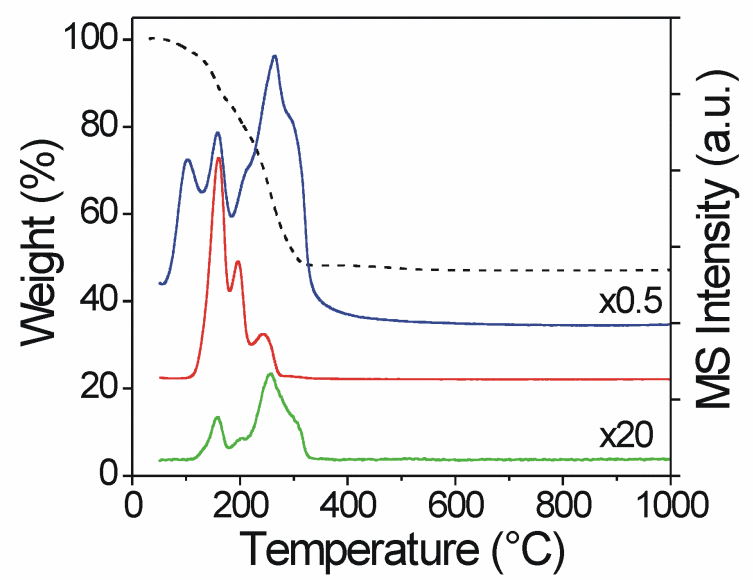

Figure S3. TGA-MS data obtained on a homogeneous mixture of $Fe(NO_3)_3 \cdot 9H_2O$ and $Cu(NO_3)_2 \cdot 3H_2O$ between 30 °C and 1000 °C in synthetic air at a heating rate of 5 °C/min. The material was prepared with no polymer template but under otherwise identical conditions. The dashed line represents the TGA curve. The MS analysis shows H_2O (m/e = 18) in blue, NO (m/e = 30) in red, and NO_2 (m/e = 46) in green. TGA indicates a mass loss of ~53 % by 1000 °C. TGA-MS shows that the thermal decomposition process begins at ~60 °C and is largely completed by 330 °C. This result is in agreement with previous studies on the thermal decomposition of various hydrated transition metal nitrates (T. Cseri, S. Bekassy, G. Kenessey, G. Liptay, F. Figueras, *Thermochim. Acta* 1996, **288**, 137; I. V. Morozov, K. O. Znamenkov, Y. M. Korenev, O. A. Shlyakhtin, *Thermochim. Acta* 2003, **403**, 173; K. Wieczorek-Ciurowa, A. J. Kozak, *J. Therm. Anal. Calorim.* 1999, **58**, 647). Both $Fe(NO_3)_3 \cdot 9H_2O$ and $Cu(NO_3)_2 \cdot 3H_2O$ are known to dissolve in their own water of crystallization below 100 °C. This process is accompanied by dehydration and formation of hydroxy nitrate species (i.e., partial hydrolysis). From TGA-MS, it can be clearly seen that both the nitrate and the formed hydroxyl groups decompose between ~110 °C and ~330 °C to NO/NO_2 and H_2O. As a result, different iron and

copper hydroxy- and oxynitrate species (i.e., $M(OH)_x(NO_3)_y$, $MO_x(NO_3)_y$, etc.) are formed, which then convert to glassy $CuFe_2O_4$.

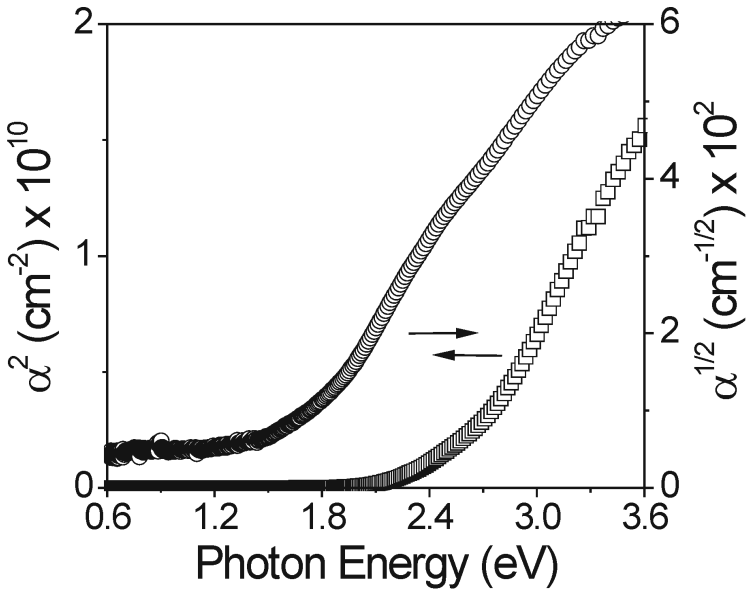

Figure S4. Plots for both direct (□) and indirect (○) optical transitions in KLE-templated $CuFe_2O_4$ spinel thin films heated to 650 °C. The following equation can be used to describe the dependence of absorption coefficient, α, on the difference between the photon energy of incident light, $h\nu$, and the band gap energy, E_g (with $h\nu > E_g$): $\alpha \propto (h\nu - E_g)^n$. In this equation, n represents the type of optical transition. For $n = 1/2$, this transition is direct while $n = 2$ indicates an indirect optical transition. We estimate the optical band gap energy from data for an indirect transition as being (1.40 ± 0.05) eV, which is in fair agreement with *ab initio* DFT calculations by Feng et al. (ref. #9 in the manuscript). In addition, we find two transitions at ~1.9 eV and ~2.5 eV, likely due to oxygen-metal charge transfer.

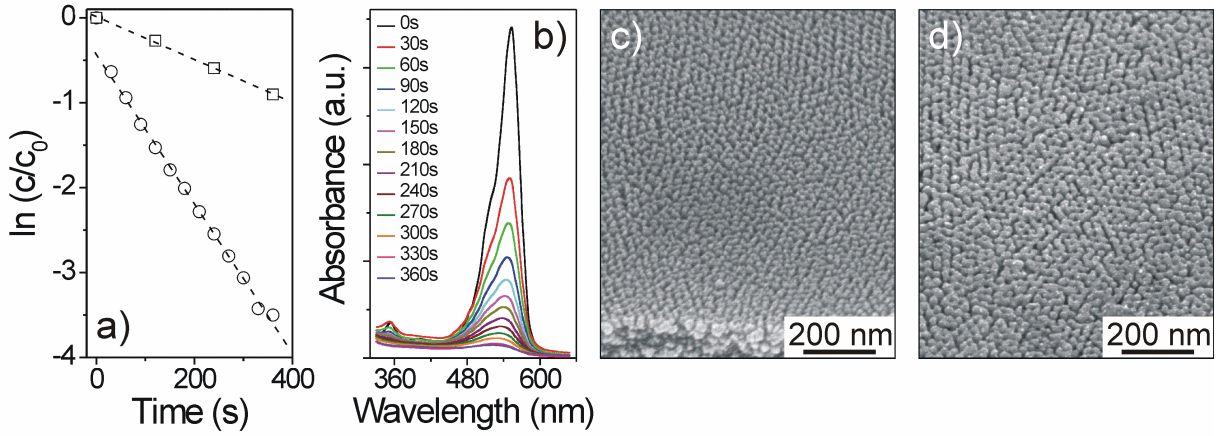

Figure S5. Photobleaching of RhB in the absence of any catalyst (□) and in the presence of a KLE-templated $CuFe_2O_4$ spinel thin film heated to 650 °C (○). (a) Semilogarithmic plots indicating that the macro-kinetics are pseudo-first-order. Dashed lines in panel (a) are linear fits to the data. From these data, it is evident that the photobleaching of RhB in the presence of H_2O_2 but with no catalyst is not negligible but significantly slower than that achieved using KLE-templated $CuFe_2O_4$. In this regard, we note that 254 nm light was used for experimental reasons, which helps explain the degradation of RhB in the absence of any photocatalyst. (b) Absorbance data collected over an exposure period of 360 s (30 s steps) in the presence of KLE-templated $CuFe_2O_4$. (c,d) SEM images at a tilt of 45° of a thin film before (c) and after (d) repeated photobleaching showing that the morphology is unaffected by experiments in aqueous solution.

In recent years, various iron-based compounds have been studied as potential heterogeneous Fenton-like catalysts for the degradation of organic pollutants. In Fenton processes, H_2O_2 is activated by iron to produce highly oxidizing hydroxyl radicals (L. Ju, Z. Chen, L. Fang, W. Dong, F. Zheng, M. Shen, *J. Am. Ceram. Soc.* 2011, **94**, 3418) - in this work, presumably in a twofold synergistic manner. First, the $CuFe_2O_4$ itself is able to produce hydroxyl radicals. Second, the photocatalytic activity of the mesoporous $CuFe_2O_4$ spinel with its large surface site

density increases the active amount of hydroxyl radicals in solution, and thus has a profound effect on the degradation rate. Lastly, we note that the materials employed here are able to maintain stable performance over several cycles as there is no decline in activity.

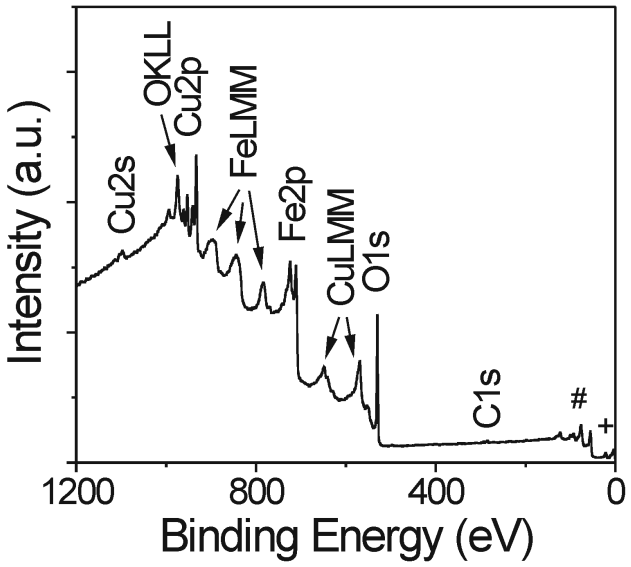

Figure S6. XPS survey spectrum of a ~175 nm thick, KLE-templated $CuFe_2O_4$ spinel film heated to 650 °C in air. The Cu3s/Fe3s/Cu3p/Fe3p and O2s core level regions are indicated by (#) and (+), respectively. Apart from a very weak carbon C1s peak, which we associate with adventitious hydrocarbon at the top surface, only copper, iron, and oxygen core levels are observed.

Table S1. XPS peak analysis data (K. Faungnawakij, N. Shimoda, T. Fukunaga, R. Kikuchi, K. Eguchi, *Appl. Catal. B-Environ.* 2009, **92**, 341; S. Poulston, P. M. Parlett, P. Stone, M. Bowker, *Surf. Interface Anal.* 1996, **24**, 811; Z. Zhou, Y. Zhang, W. Wei, W. Tang, J. Shi, R. Xiong, *Appl. Surf. Sci.* 2008, **254**, 6972).

Core level	Peak position (eV)*	Area ratio	Peak separation (eV)*
$Cu2p_{3/2}$ (oct)	933.13	0.151	2.23
$Cu2p_{3/2}$ (tet)	935.36		
$Fe2p_{3/2}$ (oct)	710.56	0.737	2.35
$Fe2p_{3/2}$ (tet)	712.91		
$Cu2p_{1/2}$ (oct)	952.81	0.154	2.27
$Cu2p_{1/2}$ (tet)	955.08		
$Fe2p_{1/2}$ (oct)	724.51	0.735	2.93
$Fe2p_{1/2}$ (tet)	727.44		

[*] error margin: ±0.05 eV

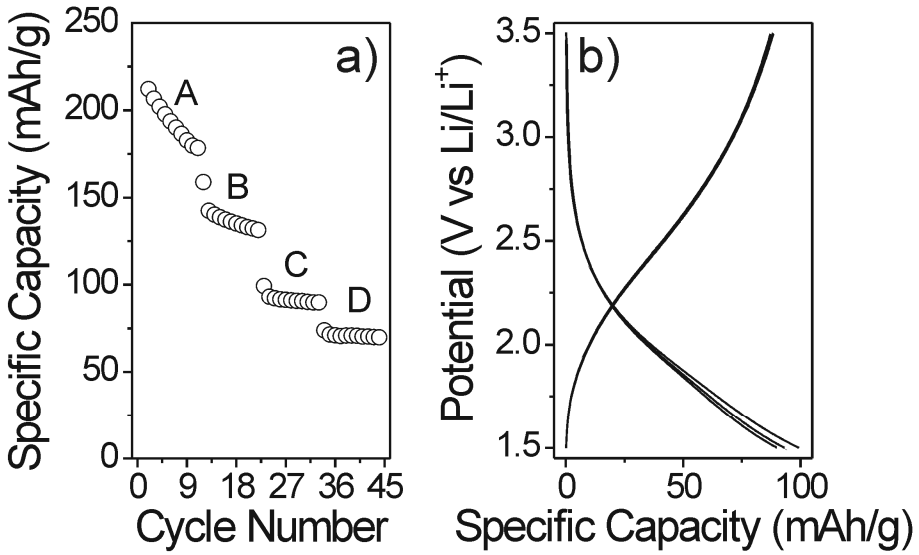

Figure S7. Charge storage characteristics of KLE-templated $CuFe_2O_4$ spinel thin films heated to 650 °C within a potential window of 3.5-1.5 V vs Li/Li^+. (a) Specific capacity as a function of cycle number for 75 $\mu A/cm^2/\mu m$ (A), 150 $\mu A/cm^2/\mu m$ (B), 300 $\mu A/cm^2/\mu m$ (C), and 600 $\mu A/cm^2/\mu m$ (D). (b) Galvanostatic charge/discharge curves for (C) in panel (a). The 1st, 5th, and 10th cycles are shown - the coulombic efficiency is close to 100 %. Overall, these data show that mesoporous $CuFe_2O_4$ thin films also have promise as electrode materials in rechargeable lithium micro-batteries. Preliminary results indicate that KLE-templated $CuFe_2O_4$ exhibits enhanced charge storage capabilities (i.e., enhanced capacity and faster charge/discharge kinetics) compared to $CuFe_2O_4$ materials described in literature (M. Bomio, P. Lavela, J. L. Tirado, *J. Solid State Electrochem.* 2008, **12**, 729; Y.-N. NuLi, Q. Z. Qin, *J. Power Sources* 2005, **142**, 292), which demonstrates that the introduction of interconnected porosity provides a beneficial microstructure for Li^+ insertion/extraction. This is likely due in part to the following: (1) short diffusion path lengths for both the electron and the cation transport, and (2) the ability of the materials to accommodate the strain associated with intercalation processes by flexing of the nanoscale pores.